The Normal Human Magnetocardiogram

II. A Multipole Analysis

PEKKA J. KARP, TOIVO E. KATILA, MATTI SAARINEN, PENTTI SILTANEN, AND TIMO T. VARPULA

SUMMARY This paper presents a multipole analysis of the QRS complex of the normal magnetocardiogram (MCG) of six normal subjects. The multipole strengths up to the octupole term were determined from the measured distribution of the z-component of the cardiac magnetic field (the component perpendicular to the frontal plane). This equivalent magnetic multipole generator was found to represent the cardiac magnetic field with a minimum error of <10%. The dipolar term of the expansion was found to represent the field distribution with reasonable accuracy early during ventricular activation, whereas late during activation, the higher multipole terms were clearly more significant.
Circ Res 47: 117-130, 1980

A THOROUGH knowledge of the normal magnetocardiogram is required before the clinical usefulness of magnetocardiography can be assessed. To gain understanding of the normal MCG, we have used two methods. A statistical analysis of the MCG morphology at 51 positions across the chest of normal subjects was presented previously (Saarinen et al., 1978). In this paper, we analyse the cardiac magnetic field of six normal human subjects in terms of the equivalent magnetic multipole sources. The data were obtained from 42–56 measurement positions.

Even complete knowledge of the electrical potential and the magnetic field everywhere outside the biological current distribution (source volume) will not allow the unique determination of the current sources, i.e., the solution of the so-called inverse problem. However, the true sources can be described in terms of different types of equivalent sources which produce the same external field and which can be solved uniquely from the measured data. Naturally, the non-uniqueness of the inverse problem cannot be circumvented, implying that the true sources cannot be uniquely solved from equivalent sources. On the other hand, a suitable equivalent generator can visualize certain features of the cardiac current distribution more easily than external magnetic field maps. Such an equivalent generator is, for instance, the multiple dipole model in which each dipole, fixed to a specific position within the heart, describes the electrical activity close to its anatomical locus. Also, if a simple equivalent generator is found that reasonably well explains the measured field values, it may have importance in the application of magnetocardiography to clinical work.

Different types of equivalent sources have been used to avoid the non-uniqueness of the MCG (and ECG) inverse problem. The simplest equivalent generator used is a dipole with time-varying orientation and magnitude but with a fixed location. In the ECG, a current dipole is used, and it forms the basis of vectorcardiography (VCG or VECG). To obtain a better fit between the measured and the predicted ECG over the chest, more complex equivalent generator arrangements have been used, based on a moving electric dipole model (Arthur et al., 1971; Horan et al., 1972), multiple electric dipole models (Fischmann and Barber, 1963), or point current multipole models (Yeh et al., 1958; Arthur et al., 1972). Geselowitz and Miller have used both magnetic and electrical data to obtain a multiple dipole inverse solution (Geselowitz and Miller, 1973; Miller and Geselowitz, 1974). Because of the clinical usefulness of the dipole model in relation to the ECG, a similar model using the magnetic dipole moment with fixed origin has also been proposed for the MCG (Baule and McFee, 1970). This model was used by Barry et al. (1977) for five normal and two abnormal subjects. The validity of this approximation has not yet been verified. Wikswo and Fairbank (1977) have used a moving magnetic dipole as the equivalent MCG source and obtained a reasonable fit to the measured data. This paper will describe the analysis of our cardiac magnetic field data in terms of the magnetic multipole expansion. To our knowledge, higher magnetic poles than the dipole have not been extracted previously from real experimental data.

From the Department of Technical Physics, Helsinki University of Technology, Espoo, Finland, and the Cardiovascular Laboratory, First Department of Medicine, Helsinki University Central Hospital, Helsinki, Finland.

Dr. Karp, Dr. Katila, and Mr. Varpula are affiliated with the Department of Technical Physics, Helsinki University of Technology, and Drs. Saarinen and Siltanen are affiliated with the Cardiovascular Laboratory, Helsinki University Central Hospital.

Address for reprints: P. Siltanen, M.D., Cardiovascular Laboratory, First Department of Medicine, Helsinki University Central Hospital, SF-00290 Helsinki 29, Finland.

Received December 13, 1978; accepted for publication December 11, 1979.

Downloaded from http://ahajournals.org by on July 27, 2019

The Magnetic Multipole Equivalent Generator

The magnetic field $\bar{B}$ at a point $\bar{r}$ produced by the total current density $\bar{j}$ at $\bar{r}'$ in the torso can be written using the Biot-Savart law:

$$\bar{B}(\bar{r}) = \frac{\mu_o}{4\pi} \int \frac{\nabla' \times \bar{j}(\bar{r}')}{|\bar{r} - \bar{r}'|} d^3r' \quad (1)$$

where integration is taken over the whole source volume. The calculation of $\bar{j}(\bar{r}')$, when the impressed cardiac current density $\bar{j}^i(\bar{r}')$ is known, is extremely difficult in the practical case, since a knowledge of electrical inhomogeneities of the torso is required (Horacek, 1973). Equation 1 shows the solution of the so-called forward problem of the MCG.

The inverse problem, i.e., the determination of $\bar{j}^i(\bar{r}')$ when the magnetic field distribution everywhere outside the torso is known, does not have a unique solution, even with the added knowledge of the electric potential everywhere on the surface of the torso (Wikswo, 1975).

To avoid the difficulties involved in the solution of the forward problem and the non-uniqueness of the inverse problem, the current sources $\bar{j}(\bar{r})$ can be represented with an equivalent generator that produces the same external magnetic field. When suitably chosen, this equivalent generator can be calculated from the measured magnetic field data. The magnetic multipole equivalent generator was used in this work. The mathematical details of this generator are presented in Appendix I.

In this model, the true cardiac sources are replaced by a set of point magnetic sources placed in the origin. The components of this set are the magnetic poles, i.e., the dipole, quadrupole, octupole, and higher poles. The magnetic field outside a sphere containing all the real sources then can be expressed as a weighted sum of dipolar, quadrupolar, octupolar, etc., fields (cf. Eq. A8). The equivalent generator parameters extracted in the multipole analysis are thus the strengths of the components of the magnetic poles, and these parameters can be uniquely calculated from the distribution of the measured magnetic field. In practice, the equivalent generator can be determined by fitting the parameters to the measured distribution with a computer. The equivalent generator based on the magnetic multipole expansion also has the advantage of being determinable from the distribution of one component of the magnetic field only. Thus, from the measurement of one component of the magnetic field, the entire vector field can be determined, if enough terms are included in the expansion.

The measurement accuracy naturally limits the number of significant terms in the expansion to a finite number. In this work, the magnetic multipole equivalent generator was evaluated up to the octupole term.

Methods

The multipole analysis was performed using the magnetocardiograms of subjects from our normal material, whose normality was carefully controlled by means of thorough clinical cardiological examination, including X-ray, resting and exercise ECG, echocardiography, and chemical and hematological laboratory investigations, as described earlier (Saarinen et al., 1978). The aims of the procedure were explained to the volunteer normal subjects, and informed consent was obtained for the studies. The superconducting magnetometer and the measurement arrangement for recording the MCG's used in this work have been described by Saarinen et al. (1974). The transducer coil of the

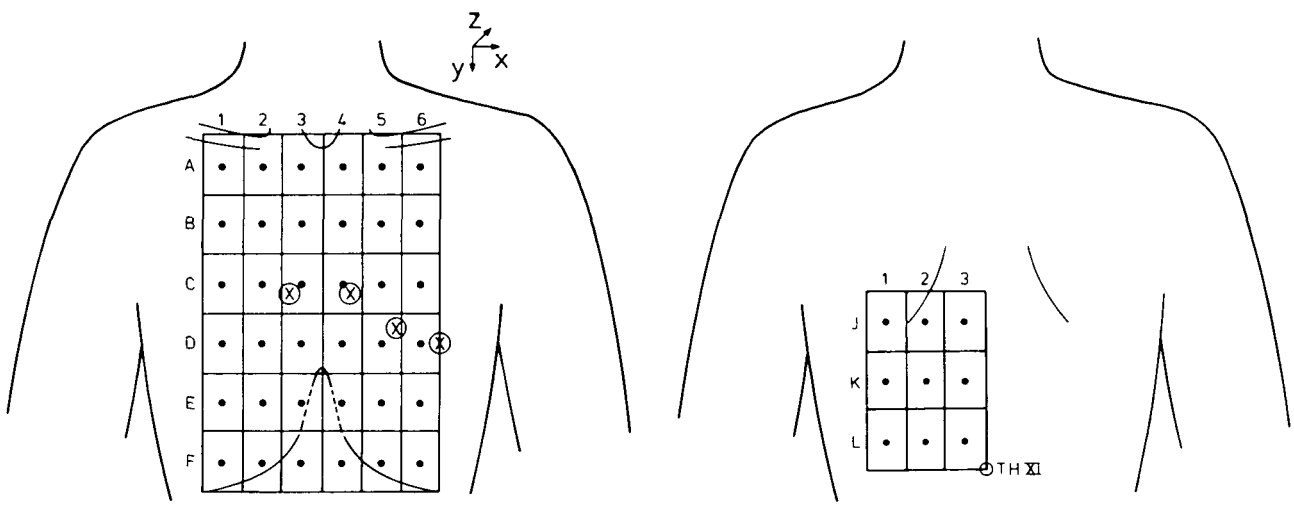

FIGURE 1 *The measurement grid and the coordinate system. The x-axis points to the left, the y-axis down, and the z-axis toward the back.*

Downloaded from http://ahajournals.org by on July 27, 2019

magnetometer used was wound in a gradiometric configuration, and the z-component (the component perpendicular to the frontal plane) of the magnetic field was measured. The measurement positions were fixed to the anatomical points of each subject according to the grid described by Saarinen et al. (1978). The number of measurement points was 45 for our subject N1, 42 with N2, 54 with N3, 49 with N4, 53 with N5, and 56 with N6. Figure 1 shows the coordinate system used in the multipole fitting. Since we are utilizing a unique set of equivalent generators of the magnetic field, in principle, the measurement arrangement has very little influence on the calculated results. A measurement bandwidth of DC to 140 Hz was used, and the MCG signal together with a simultaneous ECG lead I or II was recorded on an FM tape recorder. The ECG signal served as a timing reference.

The reproduced data from the recorder were preprocessed with a real-time minicomputer system. The MCG signals were filtered using a standard ECG bandwidth of 0.05-100 Hz. The ECG signal (lead I or II) was connected to an analog QRS-detector (Hukkinen et al., 1976) whose accuracy is about 1 msec. The detection pulses were observed with a pulse counter, connected to the

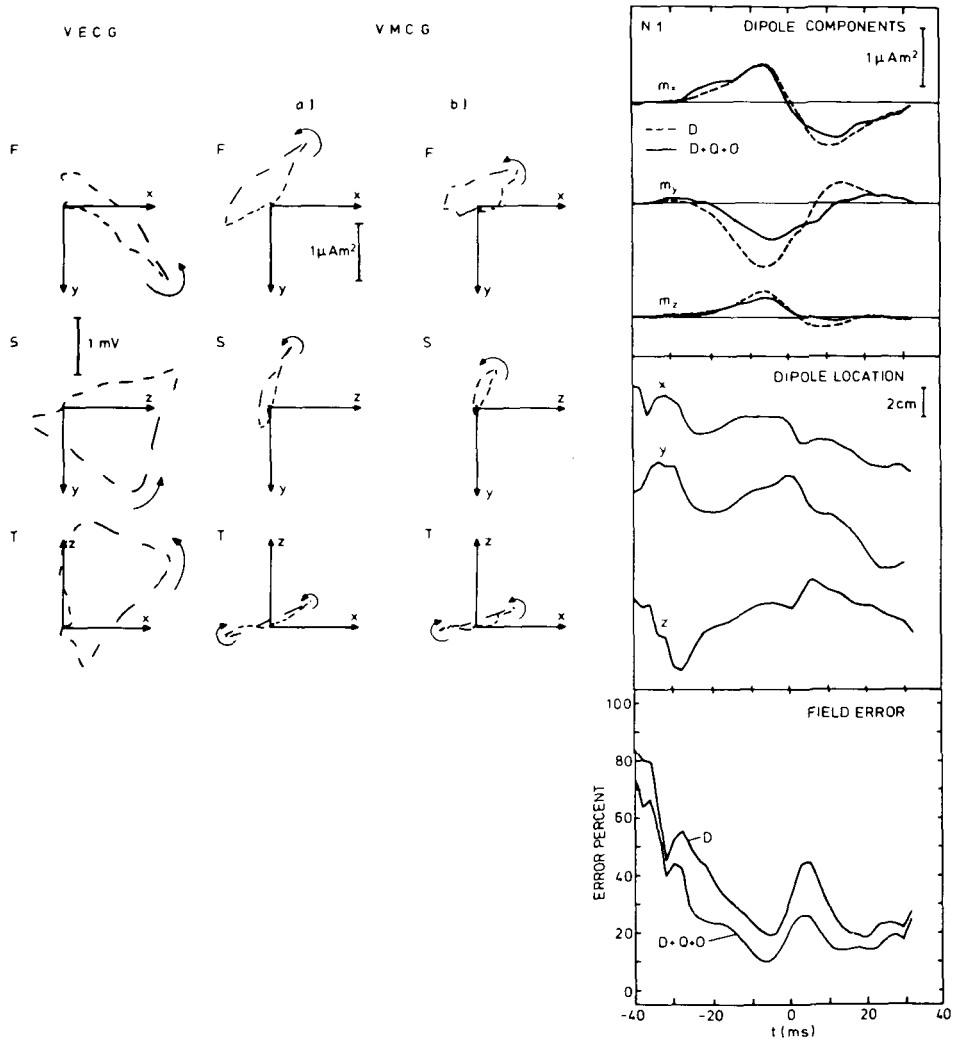

FIGURE 2 *Dipolar presentation of the electric and magnetic field of the heart during the QRS. On the left, the VECG of subject N1 is shown. The projections of the magnetic dipole loops to three orthogonal planes (VMCG) obtained from two different fitting procedures: the projections of the best-fit magnetic dipole (a) and the dipole components of the fit including the dipole plus quadrupole plus octupole (b). The length of a line element and the separation between elements is 2 msec. On the right are the best-fit magnetic dipole (broken line) and the dipole components of the fit dipole plus quadrupole and octupole (full line) as a function of time during the QRS complex. The path of the best-fit magnetic dipole is shown next and the relative error of the two fitting procedures used. The relative error is defined as:* $\{\sum_i[B_z^c(\bar{r}_i - \bar{r}_o) - B_z^m(\bar{r}_i - \bar{r}_o)]^2/\sum_i[B_z^m(\bar{r}_i - \bar{r}_o)]^2\}^{1/2}$, *where* B_z^m *is the measured and* B_z^c *the calculated field component,* $\bar{r}_i$ *is the location of one measurement, and* $\bar{r}_o$ *the origin of the magnetic multipole expansion. The zero instant in time corresponds to the peak value of the R wave in the ECG signal used for timing.*

Downloaded from http://ahajournals.org by on July 27, 2019

computer through a CAMAC dataway. The computer starts the A/D converter in the CAMAC crate when the counter receives a pulse from the QRS detector. The MCG signal was delayed to include also the P wave in the digitized complex. The sampling frequency was 500 Hz, and the length of the sample was set to 700–800 msec, depending on the heart rate of the subject. From 15 to 30 MCG complexes from each measurement position were summed up to improve the signal-to-noise ratio and the representativeness of the complex. The minicomputer averages either all complexes found with the aid of the ECG or the complexes are shown one after another for visual inspection on the display. The complexes, free of artifacts, are accepted by the operator. When the averaging has been completed, the result is punched on a paper tape for multipole fitting with a large computer.

The fitting of the magnetic poles to the digitized and preprocessed data was performed with a UNIVAC 1108 computer. The origin of the expansion was determined by fitting a moving magnetic dipole to the measured field. When a suitable origin was found, higher order poles were added to the expansion to obtain a better fit.

Determination of the best-fit magnetic dipole and the higher order poles is explained in Appendix II.

Results

The results of the multipole fits are shown in Figures 2–9. We explain first the results for normal subject N1. On the left side of Figure 2 is shown, for comparison, the vectorelectrocardiogram (VECG/Frank) of the subject. The projection planes are: F = frontal, S = sagittal, and T = transverse. The projections of the magnetic dipole loops to the three orthogonal planes (vectormagnetocardiogram, VMCG) are shown in Figure 2 and were obtained from two different fitting procedures: the projections of (a) the best-fit magnetic dipole and (b) the dipole components of the fit, including the magnetic dipole, quadrupole, and octupole.

The magnetic dipole components as a function of time, obtained from the two fitting procedures mentioned above, are also shown in Figure 2, as well as the time-dependent location of the moving magnetic center (the origin of the best-fit dipole) and the errors of the two fits. The quadrupole and octupole strengths for the same subject N1 are shown in Figure 3. Similar data for subjects N2, N5, and N6 are presented in Figures 4–9. The data for subjects N3 and N4 are not shown in figures.

Discussion

The electric dipole loops, as well as the magnetic dipole loops, from both of the fits during the QRS of four normal subjects are shown in Figures 2, 4, 6, and 8. The directions of the magnetic dipoles are in general agreement with the results obtained by Wikswo, who used a moving magnetic dipole model for the interpretation of measured vector MCG's (Wikswo 1975; Wikswo and Fairbank, 1977). The electric and magnetic dipoles are roughly orthogonal in all six cases. The sense of the magnetic dipole rotation in the loops varies with the six subjects,

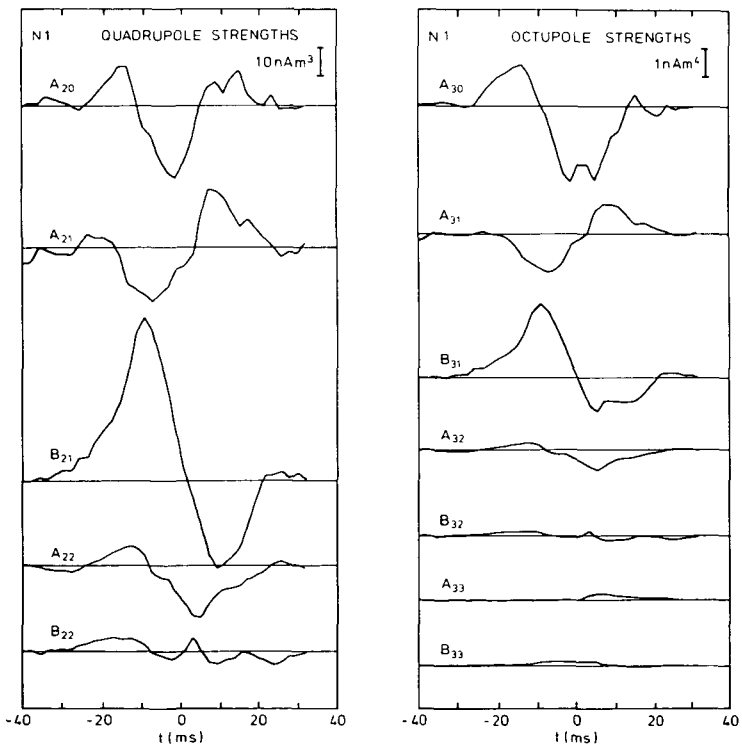

FIGURE 3 *The five quadrupole and seven octupole strengths obtained from the D + Q + O fit for subject N1 as a function of time.*

Downloaded from http://ahajournals.org by on July 27, 2019

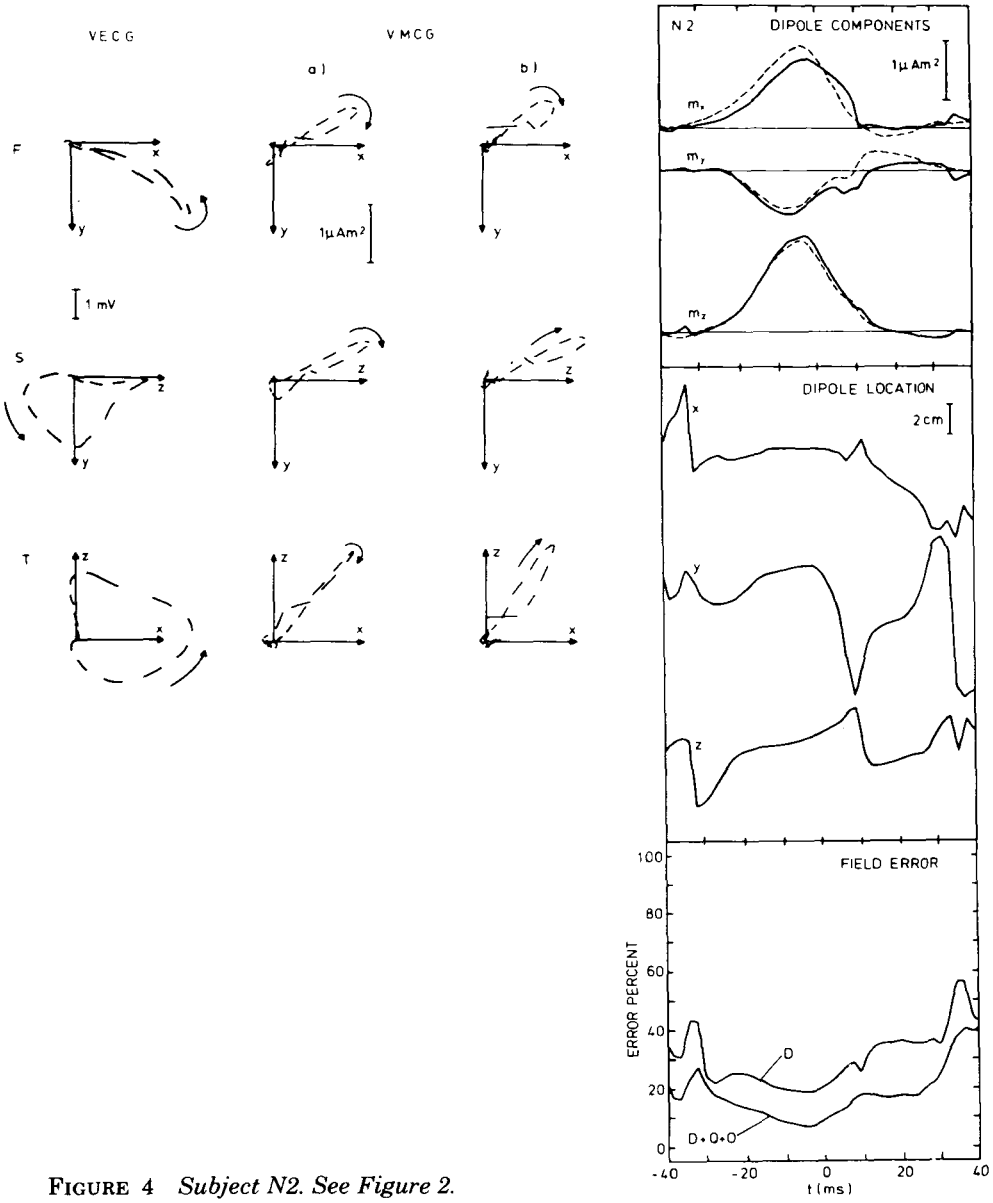

FIGURE 4 *Subject N2. See Figure 2.*

and this must be attributed to individual variability.

The magnitudes of the dipole components m_x, m_y, and m_z during the QRS are also shown in Figures 2, 4, 6, and 8 as a function of time. The zero instant in time corresponds to the peak value of the R wave in the ECG signal. The broken line represents the best-fit dipole (D) and the solid line the dipole term of the fit dipole plus quadrupole plus octupole (D + Q + O). In the limiting case of a large number of field measurements, these curves should coincide. This property is a consequence of the orthogonality of the unit fields. Here, the difference between the two curves probably is due to the limited number of field measurement points used.

The maximum dipole strengths found were 2.3 μAm^2 for subject N5 and 2.0 μAm^2 for subject N2. These values are likely to be above average, because both of the subjects had MCG complexes belonging to the 4th quartile of the magnetic field amplitude in the morphological analysis (Saarinen et al., 1978).

The errors for D and D + Q + O fits are also shown in Figures 2, 4, 6, and 8. The relative error functions, which are plotted for subjects N1 and N2 in Figures 2 and 4, reach their minima during the maximum dipole moment. This minimum of the relative error is about 20% for all six subjects when D fit is used. When D + Q + O fit is used, the minimum error is less than 10%. In all cases studied, the relative error function showed a small maximum late during the QRS, indicating the presence of higher multipoles in the field. This behavior can be explained by the known multidirectional terminal activation of the ventricular muscle mass (Durrer et al., 1970). Note that in Figures 6 and 8 the absolute error function is depicted.

The movements of the dipole origins for the

Downloaded from http://ahajournals.org by on July 27, 2019

subjects N1, N2, N5, and N6 show a similar behavior. During the time the relative error function is reasonably small (<30%), the dipole location moves smoothly. At the beginning of the QRS complex the dipole moves generally in the direction of positive coordinates, except for subject N5, in which case it moves toward the negative y-direction. During most of the QRS, the movement is confined to the yz-plane of these subjects.

The maximum speed of the dipole was 1.3 m/sec in the x-direction, 2.1 m/sec in the y-direction, and 1.5 m/sec in the z-direction. During the late QRS, the direction of the dipole is reversed, and its speed increases. This change coincides with the increasing relative error of the D fit. A similar behavior has been observed by Wikswo and Fairbank (1977). Although the path of the dipole becomes more uncertain during the late QRS due to increasing relative error, it seems to follow coarsely the activation of the left ventricle.

For our subject N3, the origin-searching algorithm for the magnetic dipole failed at two instants and, in the case of N4, at one instant of the QRS. This behavior can be explained by noting that all of the dipole moments vanished at these instants. At other instants of the QRS, the results from these subjects were reliable.

The quadrupole and octupole strengths for our six subjects are shown in Figures 3, 5, 7, and 9. These coefficients show similar features among the subjects, although this similarity is not as obvious as between the dipole strengths. The local abnormalities of the cardiac magnetic field ("proximity effect") commonly are associated with cardiac pathology. Such local fields imply the existence of strong high order poles. Therefore, the above mentioned similarity in the pattern of these higher poles might imply clinical usefulness. The quadrupole and octupole moments for the subject N2 contain abrupt changes, which clearly are connected with the failure of the origin-searching algorithm at some instants. One more common feature is that the octupole strengths for $m \geqq 2$ are small; this is due to the absence of the complicated field patterns caused by the corresponding unit fields (see Fig. A3). This feature manifests the lack of such symmetry properties in the cardiac field. Although the multipole expansion is a physically unique and complete description of the measured magnetic field distribution, it seems to contain useless components that only complicate calculations. At least for the subjects studied here, an almost equally good fit would have been obtained by omitting the multipole terms for which $m \geqq 2$, except A_{22}.

A test of the accuracy of the fit is to compare the measured field to the field calculated using the determined equivalent generator. Such a comparison is shown in Figure 10 for subject N2. The calculated and observed complexes are generally in good agreement. Also, the dipolarity of the cardiac field is manifest during the early QRS; during the late QRS, the dipolar term very often fails to explain the measured field. This happens in the area E 3–5 and B–D 5. On the other hand, the field seems to be highly dipolar in D 2–4 for this subject. The multipolarity of the field is more clearly manifest

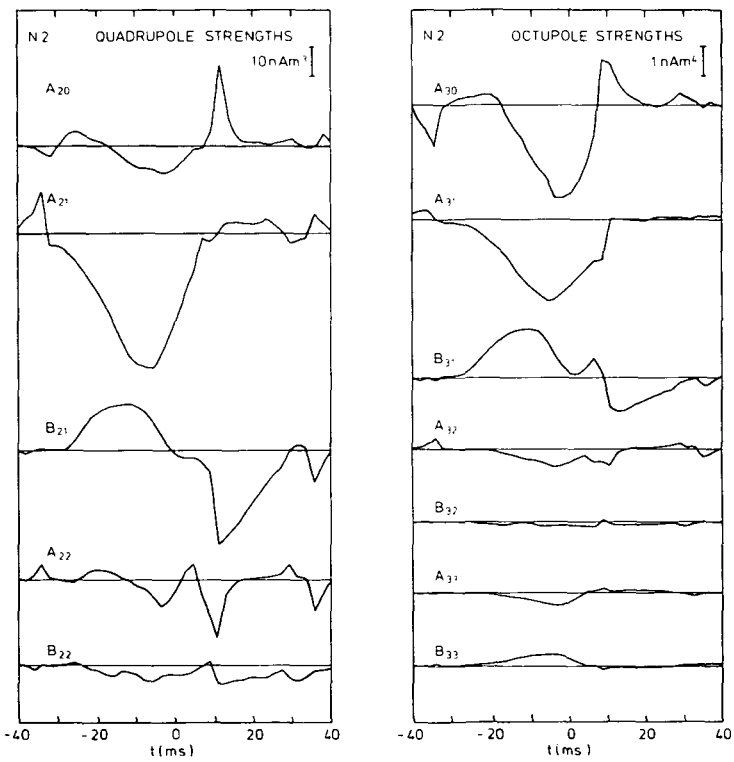

FIGURE 5 *Subject N2. See Figure 3.*

Downloaded from http://ahajournals.org by on July 27, 2019

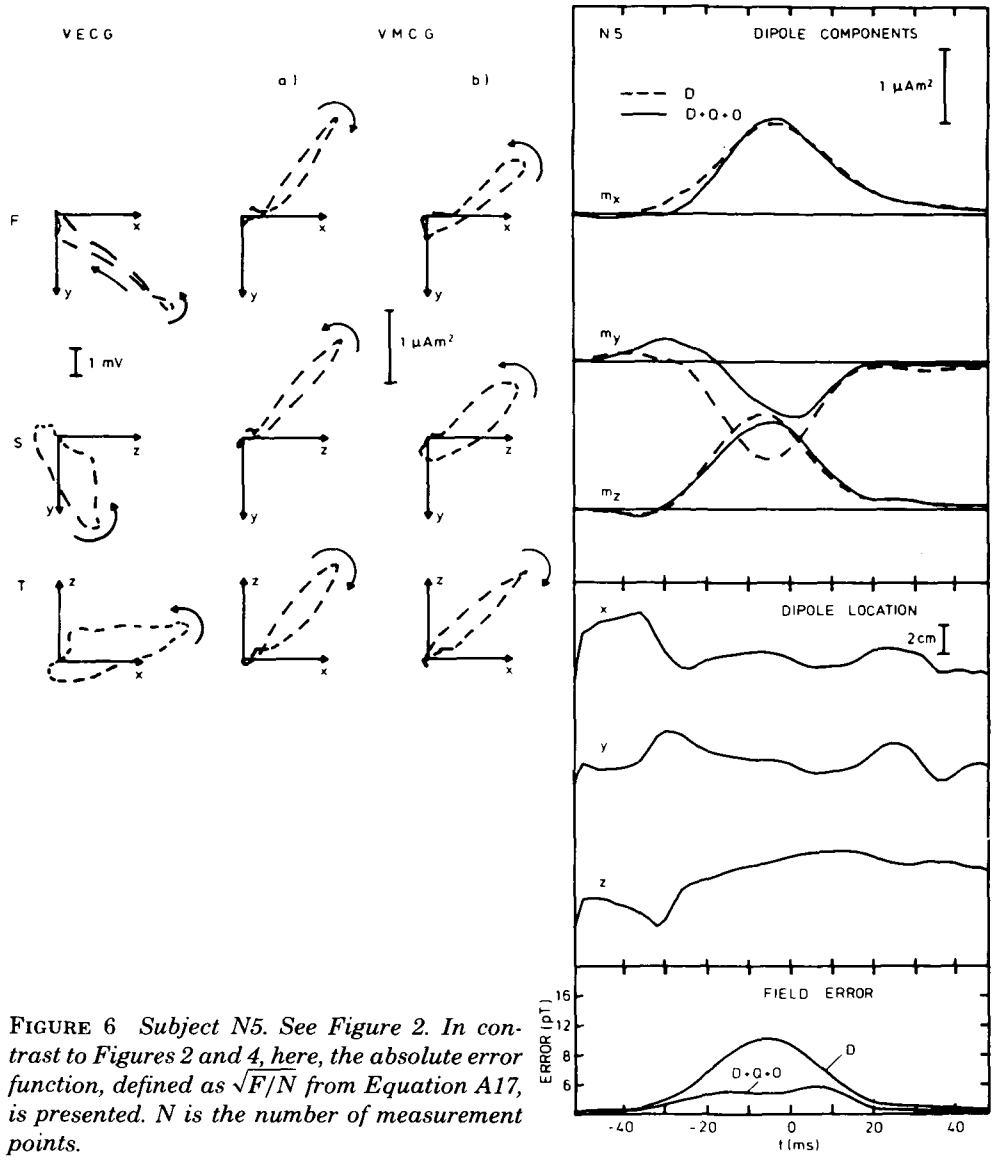

FIGURE 6 *Subject N5. See Figure 2. In contrast to Figures 2 and 4, here, the absolute error function, defined as $\sqrt{F/N}$ from Equation A17, is presented. N is the number of measurement points.*

at the posterior recording sites. Because of the faster attenuation of the quadrupolar and octupolar fields, the measurement of the dipolar term could be performed at a position which is further away from the chest wall. However, the increase in the distance between the source and the detector leads to a decrease in signal-to-noise ratio, which often is initially small. A better choice for the "dipolar" measurement positions would be ones where quadrupolar and octupolar contributions are small on the surface of the chest, because here the signal-to-noise ratio is better. The positions D 2–4, for instance, are such "dipolar" positions for subject N2 (Fig. 10). Data for more subjects must, however, be analyzed to find out whether these positions are more generally applicable.

It is very informative to construct the contour maps of the calculated field B_z^c across the chest at successive instants of time. Such contour maps from the subject N1 are shown in Figure 11, a and b. Both parts of the figure present the magnetic field at an instant of the maximum dipole strength (0 msec). Figure 11a shows the pure dipolar field caused by the best-fit magnetic dipole. Figure 11b shows the simultaneous contour map of the total calculated field. It much resembles a pure dipolar field at 0 msec. A more extensive comparison shows that, after the QRS maximum, the D + Q + O field distribution deviates remarkably from the dipolar distribution. The deviation occurs in the vicinity of the heart, which could be expected from the r^{-n-2}-dependence of the fields, where n = 1 for dipolar fields, n = 2 for quadrupolar fields, etc. (see Eq. A9).

The measurements in this work were performed with a differential magnetometer, which measures the difference of the z-component of the magnetic field across a distance of 10 cm (cf. Eq. A14). The cardiac magnetic field is not negligible at the site of the second coil. Therefore, the field seen by the

Downloaded from http://ahajournals.org by on July 27, 2019

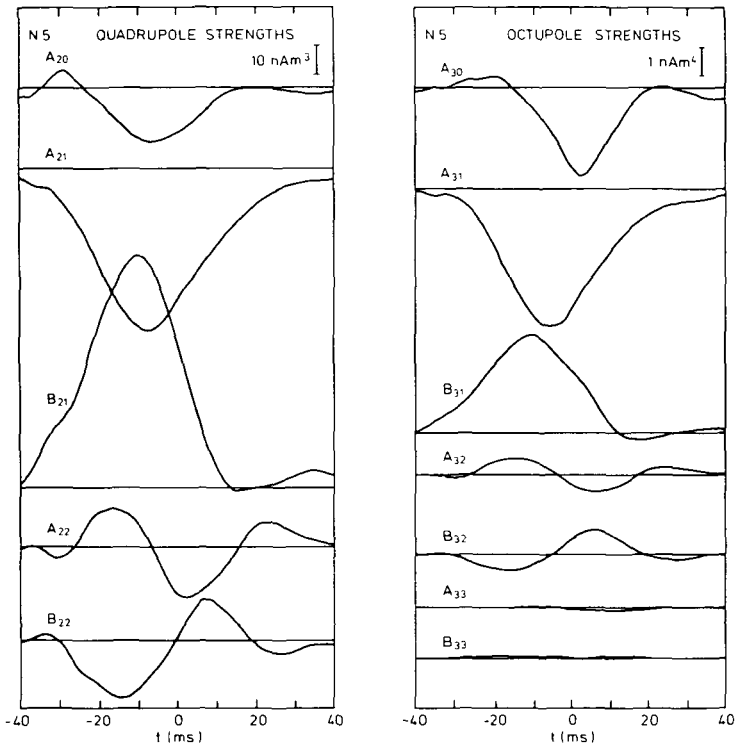

FIGURE 7 *Subject N5. See Figure 3.*

gradiometer is slightly attenuated and deformed. This effect was taken into account in the calculations.

In conclusion, the magnetic multipole expansion can be used as the equivalent generator of the cardiac magnetic field. The multipole coefficients can be determined from the spatial distribution of one component of the magnetic field only, implying that the magnetic field distribution can be completely determined from the measurement of the z-component only (see Appendix I). Thus, the z-component of the magnetic field can be determined from the distribution of any other component. This is a direct consequence of the fact that the magnetic field outside the source area can be expressed as the negative gradient of a *scalar* potential.

Appendix I

Multipole Expansion

At a point $\bar{r}$ outside the source area containing the electric currents, the magnetic field $\bar{H}(\bar{r})$ is irrotational, and hence, the quasistatic field can be expressed as the negative gradient of a magnetic scalar potential Φ_m,

$$\bar{H}(\bar{r}) = -\nabla\Phi_m(\bar{r}). \tag{A1}$$

The source of $\bar{H}(\bar{r})$ is the effective magnetic charge density $-\nabla\cdot\bar{M}(\bar{r})$ (Panofsky and Phillips, 1969). The effective magnetization $\bar{M}(\bar{r})$ is related to the total current density $\bar{j}(\bar{r})$ through:

$$\bar{M}(\bar{r}) = \tfrac{1}{2}\bar{r}\times\bar{j}(\bar{r}). \tag{A2}$$

Inside the region where the current density is non-zero, we thus obtain a Poisson's equation,

$$\nabla^2\Phi_m = \nabla\cdot\bar{M}(\bar{r}) \tag{A3}$$

which has the solution:

$$\Phi_m = -\frac{1}{4\pi}\int\frac{\nabla'\cdot\bar{M}(\bar{r}')}{|\bar{r}-\bar{r}'|}\,d^3r' \tag{A4}$$

where $\bar{r}'$ is the source point. Outside the current-carrying media $\Phi_m(\bar{r})$ is a harmonic function.

The problem is now formally equivalent to solving Laplace's equation in the electrostatic case, and the solution of Equation A3 can be written using a spherical harmonic expansion (Morse and Feshbach, 1969):

$$\Phi_m(\bar{r}) = \frac{1}{4\pi}\sum_{n=0}^{\infty}\sum_{m=0}^{n}[A_{nm}Y^e_{mn}(\theta,\phi) + B_{nm}Y^o_{mn}(\theta,\phi)]r^{-n-1} \tag{A5}$$

where

$$\left.\begin{matrix}A_{nm}\\B_{nm}\end{matrix}\right| = \epsilon_m\frac{(n-m)!}{(n+m)!}\int\bar{M}(\bar{r}')\cdot\nabla'[Y^{e,o}_{mn}(\theta',\phi')r'^n]\,d^3r' \tag{A6}$$

where ϵ_m is the Neuman factor $\epsilon_m = 1$ for $m = 0$, and $\epsilon_m = 2$ for $m \neq 0$. Note that $A_{oo} = B_{no} = 0$. The even and odd spherical harmonics are given by

$$Y^{e,o}_{mn}(\theta,\phi) = \begin{matrix}\cos\\ \sin\end{matrix}(m\phi)P^m_n(\cos\theta) \tag{A7}$$

Downloaded from http://ahajournals.org by on July 27, 2019

where $P_n^m(\cos\theta)$ is the associated Legendre function of the first kind.

The magnetic field outside the current-carrying volume can be obtained inserting the expansion (Eq. A5) into Equation A1, which yields:

$$\bar{H}(\bar{r}) = \frac{1}{4\pi}\sum_{n=0}^{\infty}\sum_{m=0}^{n}[A_{nm}\bar{H}^{e}_{mn}(\bar{r}) + B_{nm}\bar{H}^{o}_{mn}(\bar{r})] \quad \text{(A8)}$$

where $\bar{H}^{e,o}_{mn}(\bar{r})$ are the even and odd unit fields.

In deriving Equation A8, we assumed that the whole source volume can be enclosed by a sphere. Equations A5 and A8 are strictly valid only outside this sphere. The expressions of the cartesian z-components of the unit fields $\bar{H}^{e,o}_{mn}(\bar{r})$ are obtained from Equations A1, A5, A7, and A8.

$$H^{e,o}_{mn,z}(\bar{r}) = r^{-n-2}(n - m + 1) \cdot \begin{matrix}\cos\\ \sin\end{matrix}(m\phi)P^{m}_{n+1}(\cos\theta). \quad \text{(A9)}$$

Since the components of the unit fields (Eq. A9) form a complete orthogonal set on a sphere containing the sources, measurements of only one field component allow the determination of the multipole strengths A_{nm} and B_{nm}. Thus, according to Equation A8, the entire vector field $\bar{H}(\bar{r})$ is known. This determination can also be done if a field component perpendicular to a plane is measured. Some contour maps of the z-components of the dipolar, quadrupolar, and octupolar fields are shown in Figures A1 to A3. The maps have been evaluated on a plane of constant z of the rectangular coordinates.

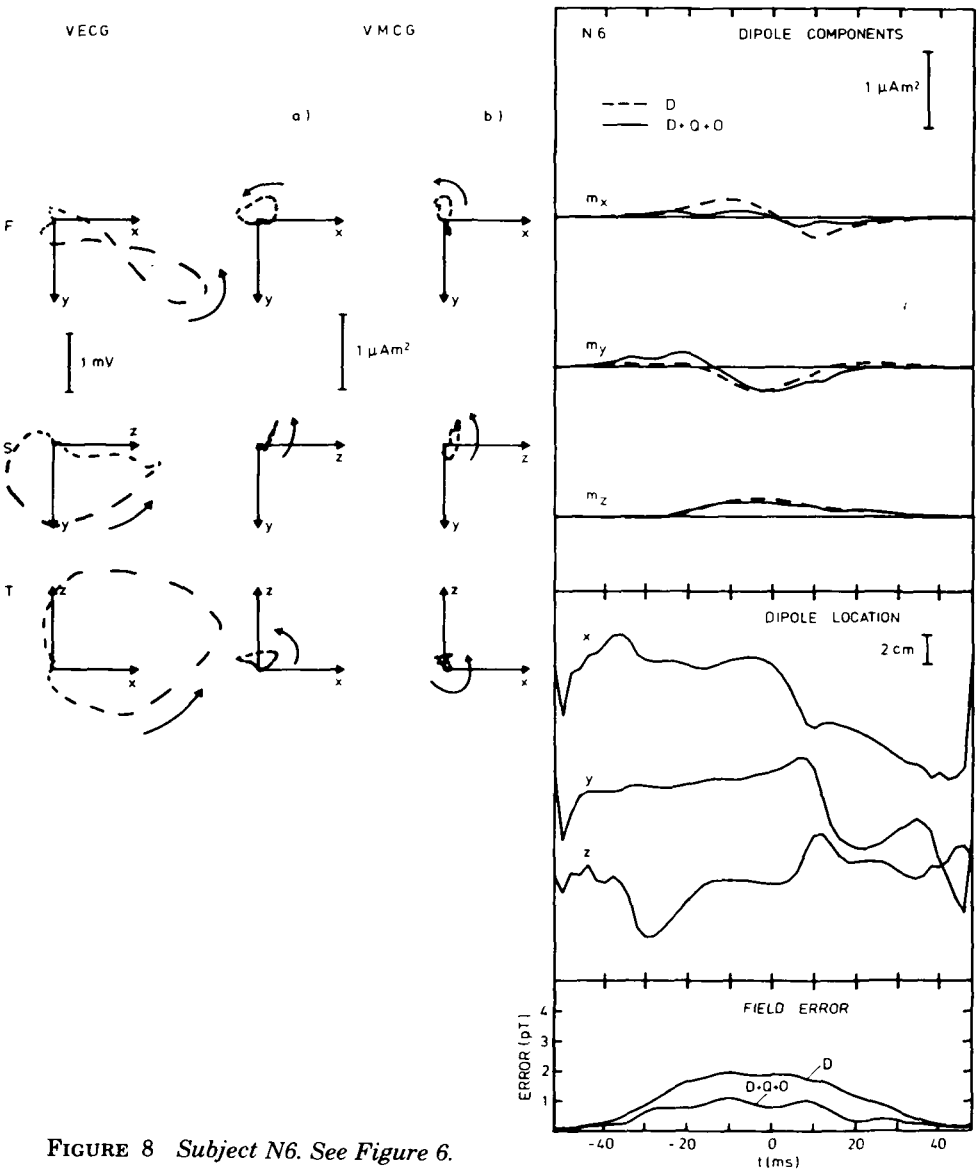

FIGURE 8 *Subject N6. See Figure 6.*

Downloaded from http://ahajournals.org by on July 27, 2019

The expressions of the coefficients A_{nm} and B_{nm} can be written directly from Equation A6. Next, we give the dipolar, quadrupolar, and octupolar coefficients in rectangular coordinates.

1. The dipole strengths:

$$\begin{pmatrix} A_{10} \\ A_{11} \\ B_{11} \end{pmatrix} = \int \begin{pmatrix} M_z(\bar{r}') \\ M_x(\bar{r}') \\ M_y(\bar{r}') \end{pmatrix} d^3r' = \begin{pmatrix} m_z \\ m_x \\ m_y \end{pmatrix} \quad \text{(A10)}$$

2. The quadrupole strengths:

$$\begin{bmatrix} A_{20} \\ A_{21} \\ B_{21} \\ A_{22} \\ B_{22} \end{bmatrix} = \int \begin{bmatrix} 2z' & -x' & -y' \\ x' & z' & 0 \\ y' & 0 & z' \\ 0 & \tfrac{1}{2}x' & -\tfrac{1}{2}y' \\ 0 & \tfrac{1}{2}y' & \tfrac{1}{2}x' \end{bmatrix} \begin{bmatrix} M_z(\bar{r}') \\ M_x(\bar{r}') \\ M_y(\bar{r}') \end{bmatrix} d^3r' \quad \text{(A11)}$$

3. The octupole strengths:

$$\begin{bmatrix} A_{30} \\ A_{31} \\ B_{31} \\ A_{32} \\ B_{32} \\ A_{33} \\ B_{33} \end{bmatrix} = \int \begin{bmatrix} \tfrac{3}{2}(2z'^2 - x'^2 - y'^2) & -3x'z' & -3y'z' \\ 2x'z' & \tfrac{1}{4}(4z'^2 - 3x'^2 - y'^2) & -\tfrac{1}{2}x'y' \\ 2x'z' & -\tfrac{1}{2}x'y' & \tfrac{1}{4}(4z'^2 - 3y'^2 + x'^2) \\ \tfrac{1}{4}(x'^2 - y'^2) & \tfrac{1}{2}x'z' & -\tfrac{1}{2}y'z' \\ \tfrac{1}{2}x'z' & \tfrac{1}{2}y'z' & \tfrac{1}{2}x'z' \\ 0 & \tfrac{1}{8}(x'^2 - y'^2) & -\tfrac{1}{4}x'y' \\ 0 & \tfrac{1}{4}x'y' & \tfrac{1}{8}(x'^2 - y'^2) \end{bmatrix} \begin{bmatrix} M_z(\bar{r}') \\ M_x(\bar{r}') \\ M_y(\bar{r}') \end{bmatrix} d^3r' \quad \text{(A12)}$$

Appendix II

Determination of the Best-Fit Magnetic Dipole

If the magnetic source is a single magnetic dipole located at the origin, the z-component of the field outside the current source can be written from Equation A8, using Equations A10 and A9.

$$B_z^{dip}(\bar{r}) = \frac{\mu_o}{4\pi}[A_{11}H^e_{11,z}(\bar{r}) + B_{11}H^o_{11,z}(\bar{r}) + A_{10}H^e_{11,z}(\bar{r})] \quad \text{(A13)}$$

$$= \frac{\mu_o}{4\pi r^5}[m_x \cdot 3xz + m_y \cdot 3yz + m_z(3z^2 - r^2)].$$

The magnetometer used in this work was a gradiometric fluxmeter. If the diameter of the measurement coils is small compared to the distance of the source from the gradiometer, we can write approximately:

$$B_z^m = k[B_z(x, y, z) - B_z(x, y, z - b)] \quad \text{(A14)}$$

where k is a proportionality coefficient, and b is the gradiometer base length. This approximation becomes worse for higher order poles because of the higher spatial frequency of unit fields with large m (cf. Eq. A9). The dependence of the measured field values B_z^m on the dipole components, with the detector function (Eq. A14) taken into account, can be written in a matrix form,

$$\underset{N}{\bar{B}_z^m} = \underset{N \times 3}{\mathbf{T}} \cdot \underset{3}{\bar{m}} \quad \text{(A15)}$$

where N is the number of measurement positions. For N = 3, $\bar{m}$ (the dipole components m_x, m_y and m_z) can be solved for the ordinary linear set of equations. It must be emphasized that the solution is correct only if the field is caused by a dipole located in the origin which is chosen for the calculation. For N > 3, the system is overdetermined, and the least square estimate of $\bar{m}$ can be computed with the aid of the pseudoinverse of the transfer matrix **T**:

$$\bar{m} = (\mathbf{T}^T\mathbf{T})^{-1}\mathbf{T}^T \cdot \bar{B}_z^m \quad \text{(A16)}$$

If the origin used in the calculations is not the true location of the dipole, the procedures yield three parameters that may not have any connection with the true dipolar term of the expansion (Eq. A8). This is a consequence of the fact that the procedures solve $\bar{m}$ for *given* $\bar{B}_z^m$ and **T**, which contain the location of the dipole. Since the origin $\bar{r}_o$ is not known a priori, the location and the magnitude of the dipole were determined using an iterative method, where a quadratic error function was minimized:

$$F = \sum_i [B_z^c(\bar{r}_i - \bar{r}_o) - B_z^m(\bar{r}_i - \bar{r}_o)]^2 \quad \text{(A17)}$$

where B_z^c is the calculated dipolar field. The minimization was performed with respect to $\bar{m}$ and $\bar{r}_o$. This dipole search was performed in two stages.

First, the Equation A15 was solved for a guessed origin using the method (Eq. A16) to supply initial values for the minimization of the error function (Eq. A17). This dipole search was performed at each time increment (2 msec apart) during the QRS.

Determination of the Higher Order Poles

Improved equivalent generators are obtained by adding quadrupole (Q) and octupole (O) terms as new parameters to be fitted. Using a fixed origin, the measured field across the chest can be written analogously with Equation A15,

$$\underset{N}{\bar{B}_z^m} = \underset{N \times 15}{\mathbf{T}'} \cdot \underset{15}{\bar{m}'} \quad \text{(A18)}$$

Downloaded from http://ahajournals.org by on July 27, 2019

Here $\bar{m}'$ includes the dipolar, quadrupolar, and octupolar strengths. The origin of the best-fit dipole $\bar{r}_0$ was chosen as the origin of the dipole plus quadrupole plus octupole (D + Q + O) solution. The set of Equations A18 was inverted using the pseudoinverse technique (Eq. A16), and the procedure yielded the multipole strengths.

Acknowledgments

We thank the Academy of Finland, the Juselius Foundation, and the Heart Research Foundation for their financial support. We would also like to thank Professor P.I. Halonen and Professor E. Byckling for their support and valuable suggestions. Finally, the assistance of K. Aittoniemi and M.-L. Järvinen during the analysis of the data is gratefully acknowledged.

References

Arthur RM, Geselowitz DB, Briller SA, Trost RF (1971) The path of the electrical center of the human heart determined from surface electrocardiograms. J Electrocardiol **4:** 29–33

Arthur RM, Geselowitz DB, Briller SA, Trost RF (1972) Quadrupole components of the human surface electrocardiogram. Am Heart J **83:** 663–677

Barry WH, Fairbank WM, Harrison DC, Lehrman KL, Malmivuo JAV, Wikswo JP Jr (1977) Measurement of the human magnetic heart vector. Science **198:** 1159–1162

Baule GM, McFee R (1970) The magnetic heart vector. Am Heart J **79:** 223–236

Durrer D, van Dam RTh, Freud GE, Janse MJ, Mejler FL, Arzbaecher RC (1970) Total excitation of the isolated human heart. Circulation **41:** 899–912

Fischmann EJ, Barber MR (1963) 'Aimed' electrocardiography. Model studies, using a heart consisting of 6 electrically isolated areas. Am Heart J **65:** 628–637

Geselowitz DB, Miller WT (1973) Extracorporeal magnetic fields generated by internal bioelectric sources. IEEE Trans Magn *MAG*-**9:** 392–398

Horacek BM (1973) Digital model for studies in magnetocardiography. IEEE Trans Magn *MAG*-**9:** 440–444

Horan LG, Flowers NC, Miller CB (1972) A rapid assay of dipolar and extradipolar content in the human electrocardiogram. J Electrocardiol **5:** 211–223

Hukkinen K, Katila, TE, Laine H, Lukander R, Mäkipää P, Kariniemi V (1976) Instantaneous fetal heart rate monitoring by electromagnetic methods. Am J Obstet Gynecol **125:** 1115–1120

Miller WT, Geselowitz DB (1974) Use of electric and magnetic data to obtain a multiple dipole inverse cardiac generator: A spherical model study. Ann Biomed Eng **2:** 343–360

Morse PM, Feshbach H (1969) Methods of Theoretical Physics, vol 2. New York, McGraw-Hill, pp 1252–1308

Panofsky WKH, Phillips M (1969) Classical Electricity and Magnetism. Reading, Massachusetts, Addison-Wesley, pp 140–144

Saarinen M, Karp PJ, Katila TE, Siltanen P (1974) The magnetocardiogram in cardiac disorder. Cardiovasc Res **8:** 820–834

Saarinen M, Siltanen P, Karp PJ, Katila TE (1978) The normal magnetocardiogram: I. Morphology. Ann Clin Res **10** (suppl 21): 1–43

Wikswo JP Jr (1975) Non-invasive magnetic measurement of the electrical and mechanical activity of the heart. Thesis, Stanford, Stanford University

Wikswo JP Jr, Fairbank WM (1977) Application of superconducting magnetometers to the measurement of the vector magnetocardiogram. IEEE Trans Magn *MAG*-**13:** 354–357

Yeh GCK, Martinek J, de Beaumont H (1958) Multipole representations of current generators in a volume conductor. Bull Math Biophys **20:** 203–216

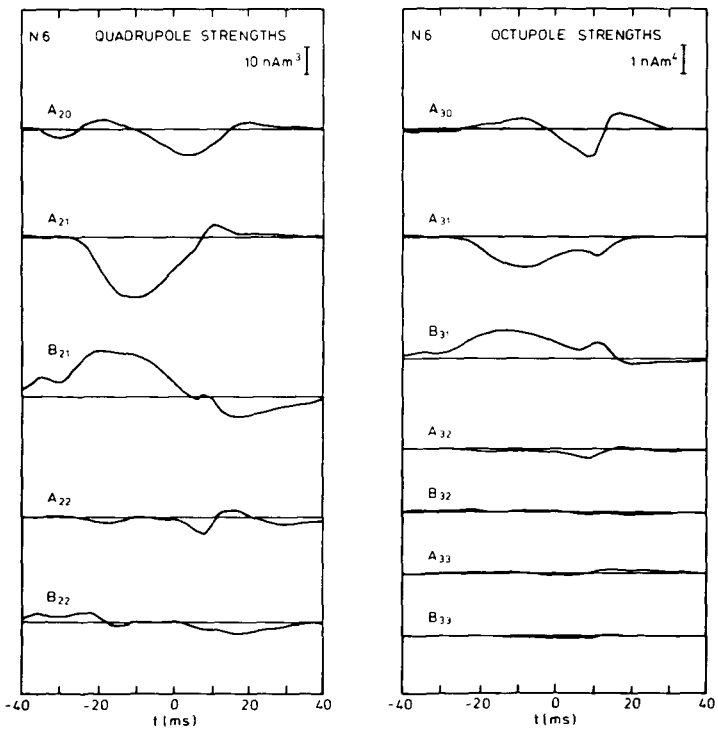

FIGURE 9 *Subject N6. See Figure 3.*

Downloaded from http://ahajournals.org by on July 27, 2019

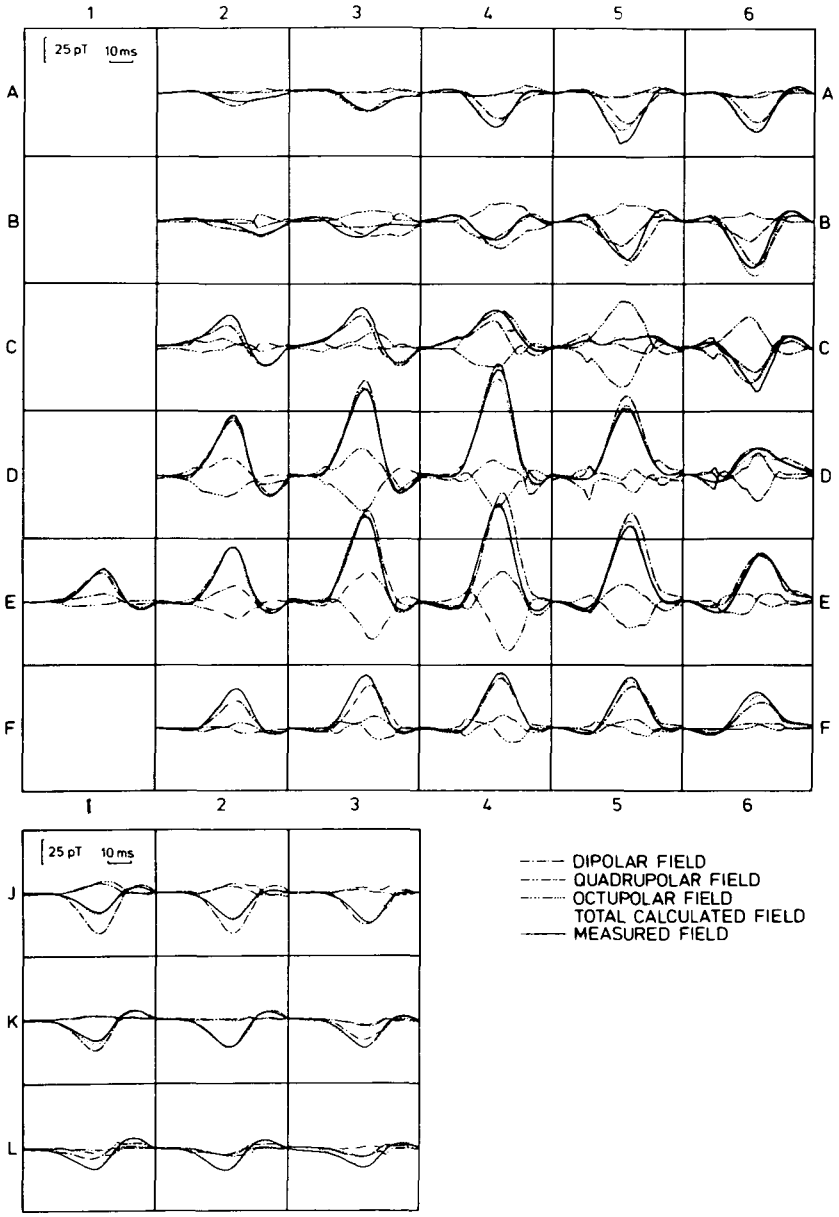

FIGURE 10 *Comparison between the measured and the calculated MCG complexes across the chest of a normal subject. The figure shows also the individual contributions of the D, Q, and O terms. The position E1 was not used when the fitting of the poles was performed. Hence, it can be used as a test of the accuracy of the method.*

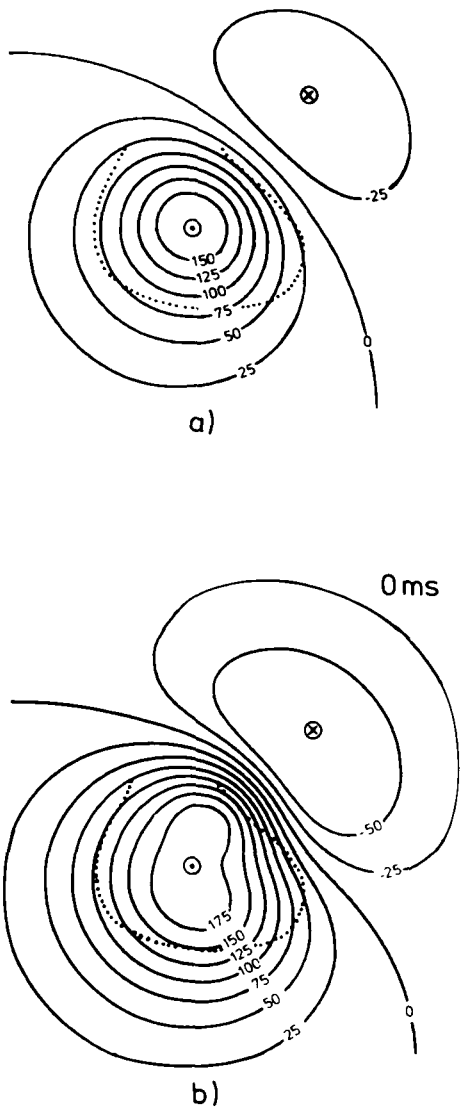

FIGURE 11 *Contour maps of the cardiac magnetic field across the anterior chest at the instant of the maximum QRS of the cardiac cycle for a normal subject, N2 (0 msec = peak QRS). The maps were determined from the calculated multipole components. The field strength is expressed in picotesla. The broken line shows the outline of the frontal cardiac silhouette. (a) The pure dipolar field. (b) The total calculated multipole field.*

Downloaded from http://ahajournals.org by on July 27, 2019

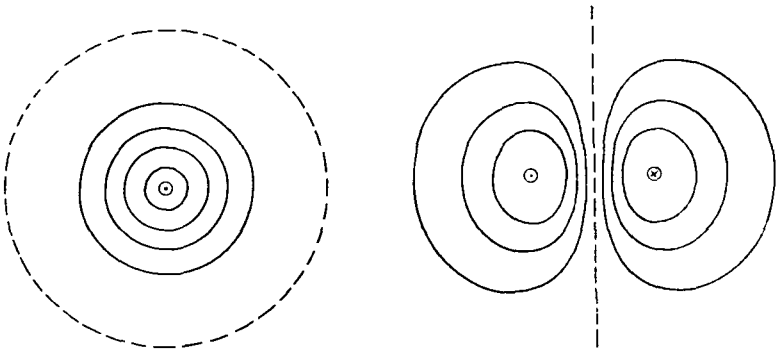

$H^{E}_{01,z} = (3z^2-R^2)R^{-5}$ $H^{E}_{11,z} = 3xzR^{-5}$

FIGURE A1 *The field contour maps of the z-components of the dipolar unit fields, evaluated on a plane parallel to the xy-plane. Note that the unit field $H^{o}_{11,z}$ is obtained from $H^{e}_{11,z}$ by a rotation of 90° around the z-axis. The broken lines show the zero-field contour.*

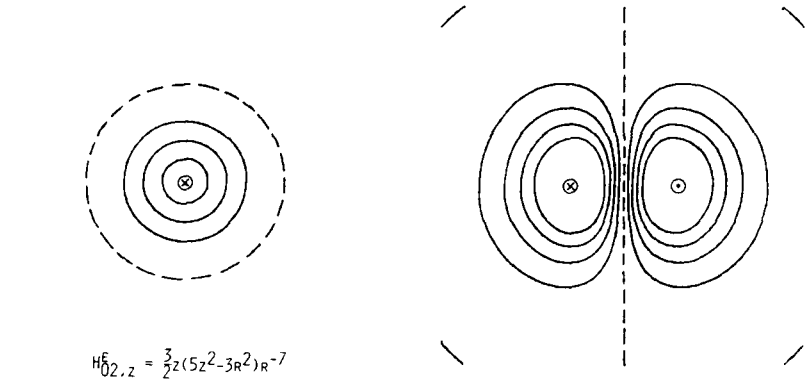

$H^{E}_{02,z} = \frac{3}{2}z(5z^2-3R^2)R^{-7}$ $H^{E}_{12,z} = 3x(5z^2-R^2)R^{-7}$

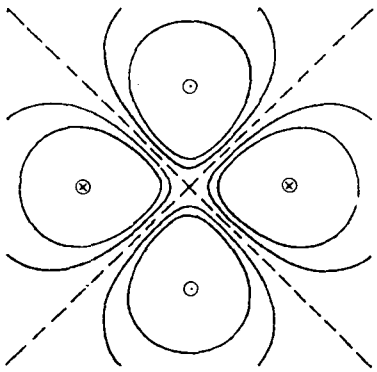

$H^{E}_{22,z} = 15z(x^2-y^2)R^{-7}$

FIGURE A2 *The field contour maps of the z-components of the quadrupolar unit fields. Note that the odd unit field $H^{o}_{12,z}$ is obtained by a rotation of 90° and the odd unit field $H^{o}_{22,z}$ by a rotation of 45° around the z-axis from the corresponding even unit fields. The broken lines show the zero field contour.*

Downloaded from http://ahajournals.org by on July 27, 2019

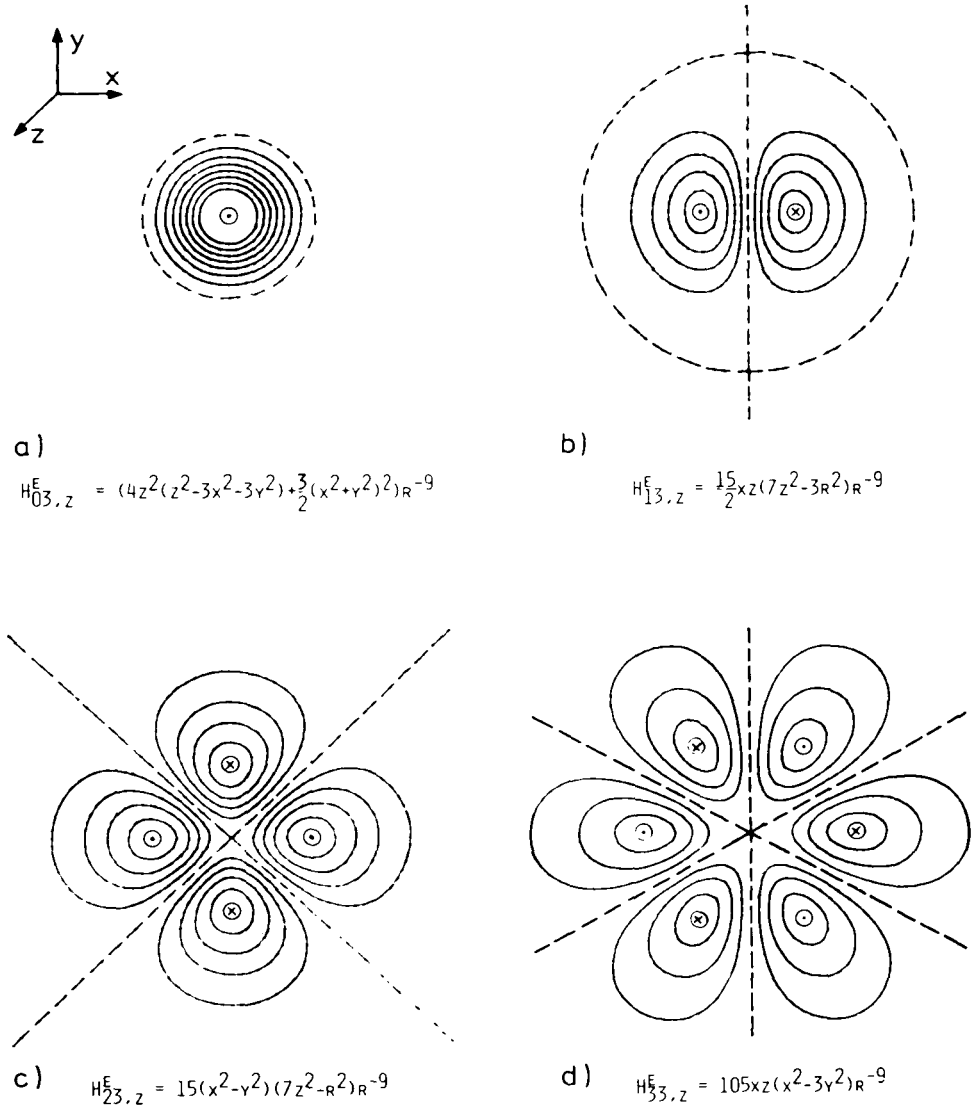

FIGURE A3 *The field contour maps of the z-components of the octupolar unit fields. Note that the odd unit fields $H^o_{13,z}$ and $H^o_{33,z}$ are obtained by a rotation of 90° and the odd unit field $H^o_{23,z}$ by a rotation 45° around the z-axis from the corresponding even unit fields. The broken lines show the zero field contour.*

Downloaded from http://ahajournals.org by on July 27, 2019